Pis'ma v ZhETF, vol. 102, iss. 12, pp. 911 – 918

Anharmonic Bloch oscillation of electrons in biased superlattices

K. A. Ivanov[+*], *A. G. Petrov*[×], *M. A. Kaliteevski*[+*×1)], *A. J. Gallant*[°]

[+]*St. Petersburg Academic University, 194021 St. Petersburg, Russia*

[*]*St. Petersburg National Research University of Information Technologies, Mechanics and Optics, 197101 St. Petersburg, Russia*

[×]*Ioffe Physico-Technical Institute of the RAS, 194021 St. Petersburg, Russia*

[°]*School of Engineering and Computing Sciences, Durham University, South Road, DH1 3LE Durham, UK*

Submitted 2 September 2015

The oscillatory motion of electrons in a periodic potential under a constant applied electric field, known as Bloch Oscillations (BO), is one of the most striking and intriguing quantum effects and was predicted more than eighty years ago. Oscillating electrons emit electromagnetic radiation and here we consider this BO effect for emission in the THz region. To date, it has been assumed that the Bloch oscillation of an electron is an harmonic oscillation, therefore with radiation emitted at the single Bloch frequency. We analyze scenarios when Bloch oscillations can be accompanied by the emission of radiation not only at the Bloch frequency but also with double and triple Bloch frequencies. The first scenario means that electrons could jump over neighboring Stark states. The second scenario of anharmonic emission is coupled to an opening of the minigap in the miniband.

DOI: 10.7868/S0370274X15240030

Introduction. When an electric field F is applied to an electron in a periodic potential with a period d, its translational motion can be transformed into an oscillatory motion [1, 2] with a frequency ω given by

$$\hbar\omega = eFd, \tag{1}$$

where e is the electron charge.

For a one-dimensional periodic potential, the dependence of the electron energy on its wavevector, K is also periodic. When the electron, experiencing acceleration under an applied electric field reaches the energy corresponding to an inflection point of the dispersion dependence, the effective mass of the electron becomes negative, and its group velocity starts to fall with subsequent increase of its energy. When an electron reaches the edge of Brillouin zone, its group velocity changes sign and the electron starts to move back. Such oscillatory motion, called Bloch oscillation (BO), implies that the electron reaches the energy, corresponding to the top of the band, which defines the threshold values of electric field F_{th} [3, 4]

$$W = eF_{th}l, \tag{2}$$

where W is a width of energy band and l is a mean free path of an electron.

The oscillatory motion of an electron should be accompanied by the emission of electromagnetic radiation with the frequency defined by Eq. (1). A more accurate picture of BO can be given by the following quantum mechanical consideration. When an electric field is superimposed on a periodic potential, the miniband structure is replaced by the set of equidistant localized states (called Stark states) separated by the energy interval given by Eq. (1): Wannier–Stark localization occurs [5, 6], as shown in Fig. 1a. In the framework of this picture, electromagnetic radiation is emitted via spa-

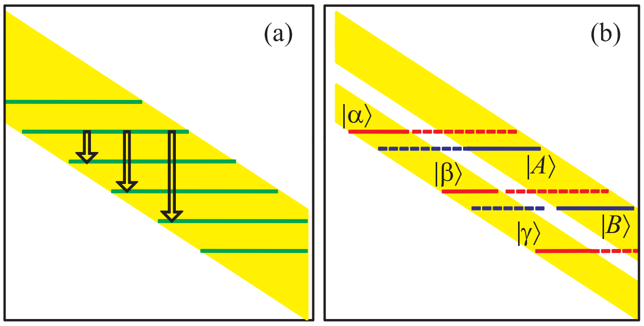

Fig. 1. (Color online) (a) – Schematic picture of Wannier–Stark ladder in the miniband of a biased superlattice. Arrows indicate transitions between the neighboring states (separated by Bloch energy), and jumps over one and two Stark states (separated by double and triple Bloch energies, respectively). (b) – Miniband in biased superlattice split with a gap of width D. The states $|\alpha\rangle$, $|\beta\rangle$, and $|\gamma\rangle$ are localized mostly in lower sub-miniband while the states $|A\rangle$ and $|B\rangle$ are localized mostly in upper sub-miniband

[1)]e-mail: mkaliteevski@gmail.com

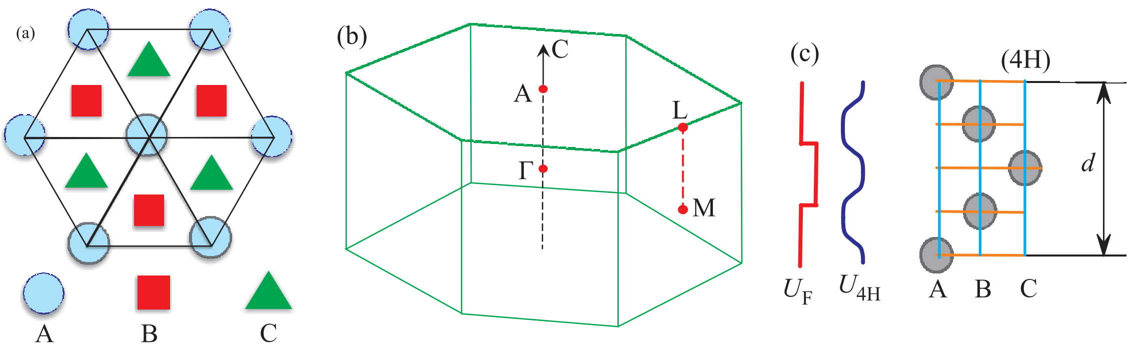

Fig. 2. (Color online) (a) – Arrangements of atoms in the densely packed layers. (b) – Brillouin zone of hexagonal crystalline lattice. Axis C is an axis of natural SL in SiC. Arrangement of atomic layers (Ramsdell zigzag) for the polytype 4H–SiC (c). The circles denote a pair of atoms Si–C. (c) – The component of 1D potential profile along axis of symmetry C (with the period equal to half-period of structure), introduced by Dubrovski et al. [26] for the description of the properties of SiC natural superlattices, denoted as $U_{4\mathrm{H}}$. An additional 1D potential (with the period equal to the period of structure) leads to the appearance of the minigap, denoted as U_{F}

tially indirect radiative transitions between states in the so-called Stark ladder.

In most natural crystals, observation of BO is practically impossible due to the large bandwidth, which requires very strong electric fields exceeding the breakdown limits. In 1970, in the pioneering work of Esaki and Tsu [7], artificial superlattices (SL) with a miniband energy spectrum were suggested as a prospective basis for the development of THz radiation emitters. Some unambiguous precursors of BO such as negative differential conductivity caused by Bragg scattering of electrons [8, 9], Bloch gain [10, 11]. Stark localization [12, 13] have been demonstrated experimentally. Furthermore, some evidence of BO and its corresponding THz radiation were obtained by optical techniques in artificial superlattices (SL) which were electrically biased and under band–to band excitation by femtosecond laser pulses [4, 14, 15].

There are also natural SLs occurring in silicon carbide [16–18]. The crystalline lattice of silicon carbide can be (similarly to the case of GaAs or Si) considered as a stack of densely packed layers. In contrast to an arrangement of the type ABCABC (for zincblende structures) or ABAB (for wurtzite structures) type, the arrangement of layers for different polytypes is more complicated: the polytype 4H–SiC has an elementary unit such as ABCB, as illustrated in Fig. 2. Existence of a period, equal to several spacings between layers leads to the formation of miniband structure in a SiC natural SL [18], as shown in Fig. 2. Recently, emission of THz radiation with emission power of over 10 μW from quasi-CW biased 6H–SiC at liquid helium temperatures has been experimentally observed [19].

Hexagonal polytypes of SiC, have a peculiar band structure in the vicinity of the minima, closest of the Fermi level for the direction corresponding to an axis of symmetry of the structure C [20]. Note that the Bloch oscillation in SiC was observed for the motion of the electrons along C. On the boundary of the Brillouin zone, the state in symmetry point L is twice degenerated and folding of the dispersion dependence occurs [20]. Therefore, for the wavevector, K in 1st Brillouin zone, in the interval between $\bar{\mathrm{L}}$ and L (for $-\pi/d < K < \pi/d$), the electron effective mass in the lower branch of dispersion dependence is positive, and no oscillatory motion is possible (see Fig. 2). The inflection point of dispersion dependence required to change the sign of group velocity of electron corresponds to wavevector, K lying within the intervals $-2\pi/d < K < -\pi/d$ and $\pi/d < K < 2\pi/d$, as shown in Fig. 3a.

Therefore, the electron cannot experience Bragg reflection when it reaches the edge of the 1st Brillouin zone at the L point. In other words, without a bandgap (at the L point), no Bragg reflection occurs. On other hand, the electron can be reflected at the edge of the 2nd Brillouin zone at point M with $K = 2\pi/d$. Thus, the BO in K-space along is characterized by a period of $4\pi/d$ and is associated not with the full period in real space, but with its half-period, $d/2$. Such motion of the electron experiencing the cycle of Bloch oscillation, shown in Fig. 3a, is accompanied by a radiation emission with the frequency $\omega = eFd/(2\hbar)$. If the degeneracy L point is lifted (due to application of the stress, magnetic of electric field), a minigap appears, and inflection point of dispersion relation occurs in the 1st Brillouin zone. In this case the period of BO in K-space have a period which becomes equal to $2\pi/d$, corresponding to the period of the crystal in real space d. Such motion is accompanied by emission of the radiation with the frequency $\omega = eFd/\hbar$. At the same time, electrons can

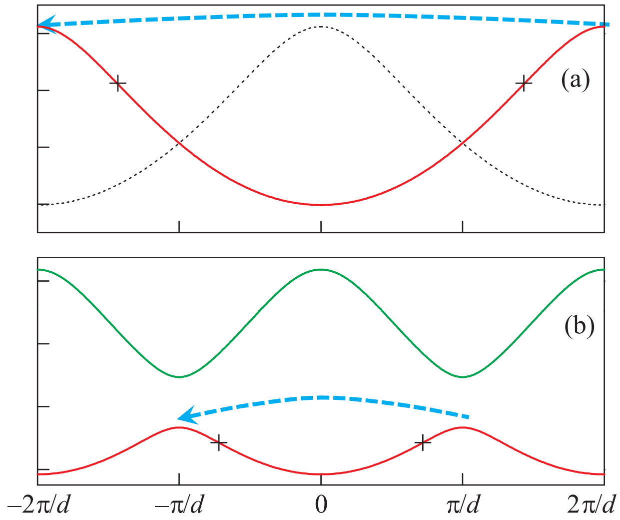

Fig. 3. (Color online) The dispersion relations in the model 1D potential, corresponding to a fragment of the dispersion relation for natural non-biased SL 4H–SiC along MЧL line, expressed using Jones zone scheme in the vicinity of indirect minimum in conduction band (closest to the Fermi level) in the absence (a) and presence (b) of a superimposed potential with double period. Arrows illustrate the process of Bloch oscillations for two cases. The period of natural superlattice denoted as d. The crosses mark the inflection points on the dispersion relations

tunnel through the minigap, and have the trajectory in K-space shown in Fig. 3b. Thus, a co-existence of the BO of an electron with different spatial periods (which differs by factor of 2) occurs. This effect could lead to simultaneous emission of radiation with single and double Bloch frequencies.

At present, it is assumed that the BO of electrons in a SL is a harmonic oscillation, accompanied by emission of radiation with single frequency, defined by Eq. (1). Detailed analysis of the dynamics of electrons has been provided by Luban et al. [21, 22] using nearest neighbor approximation, and in the framework of this approach it was shown that dipole matrix element is nonzero only for the transition between neighboring Stark states, separated by the Bloch energy given in Eq. (1). On the other hand, the spatial profile of the potential, providing Wannier–Stark localization differs substantially from the parabolic potential, leading to harmonic oscillation, and one might expect that the matrix elements, corresponding to radiative transitions between Stark states separated multiple Bloch energies could also have non-zero values. In addition, some manifestations of non-linear properties of Bloch oscillation were demonstrated theoretically [23] and experimentally [24, 25].

This paper is aimed at the investigation of the possibility of radiation emission with double, triple, and multiple Bloch frequencies originated from BO. First, the possibility of a multiple frequency emission caused by anharmonicity of BO will be analyzed. After which the influence of the minigap in the electron band on the motion of electron and emission of radiation will be studied.

We use effective media approach and 1D potential, which initiate a miniband in the dispersion relation, similar to the miniband in SiC, which is responsible for recently observed BO [19]. For the modeling, we use a finite size SL, formed by 100 quantum wells each with a thickness of 0.57 nm separated by barriers with a thickness of 0.33 nm. The height of the barrier is 2 eV. The resulting SL has a period of 0.9 nm and possesses a miniband with the width of 600 meV, as shown in Fig. 3. Such a 1D potential, denoted as $U_{4\mathrm{H}}$ in Fig. 2c was proposed by Dubrovski [26, 27] for the modeling of a natural SL based on SiC. Such a very simplified model potential provides an adequate description of the experimentally observed optical [28] and electrical [29] properties of silicon carbide. The total thickness of the SL is 80 nm, and it is surrounded by barriers with a height of 2 eV. Despite the simplicity of the effective media model, the chosen 1D potential represents the principal features of the branch in dispersion relation for SiC, in the vicinity of a minimum at the M point, which is closest to Fermi level (see Fig. 2f in Ref. [20]). In particular, the 1D potential model yields a similar miniband width, which is responsible for BO in SiC, and also the shape of the dispersion relation for this minigap. Furthermore, the effect of minigap opening can be modeled simply by superimposing an additional potential U_{F} with doubled period (see Fig. 2c).

Results and discussion. The Stark states and their wavefunctions were obtained by the "outgoing wave approach" [30], utilizing the transfer matrix technique to solve the Schrödinger equation (see the Appendix for details).

Fig. 4 shows the profiles of the probability density for the Stark states, localized in a biased superlattice for different values applied electric fields. The value of the applied field defines the frequency of Bloch oscillations.

It can be seen that the Stark states have a characteristic size s, given by

$$s = W/eF \tag{3}$$

corresponding to the cross-section of the sloped miniband by the equipotential line and rapidly decays outside the miniband.

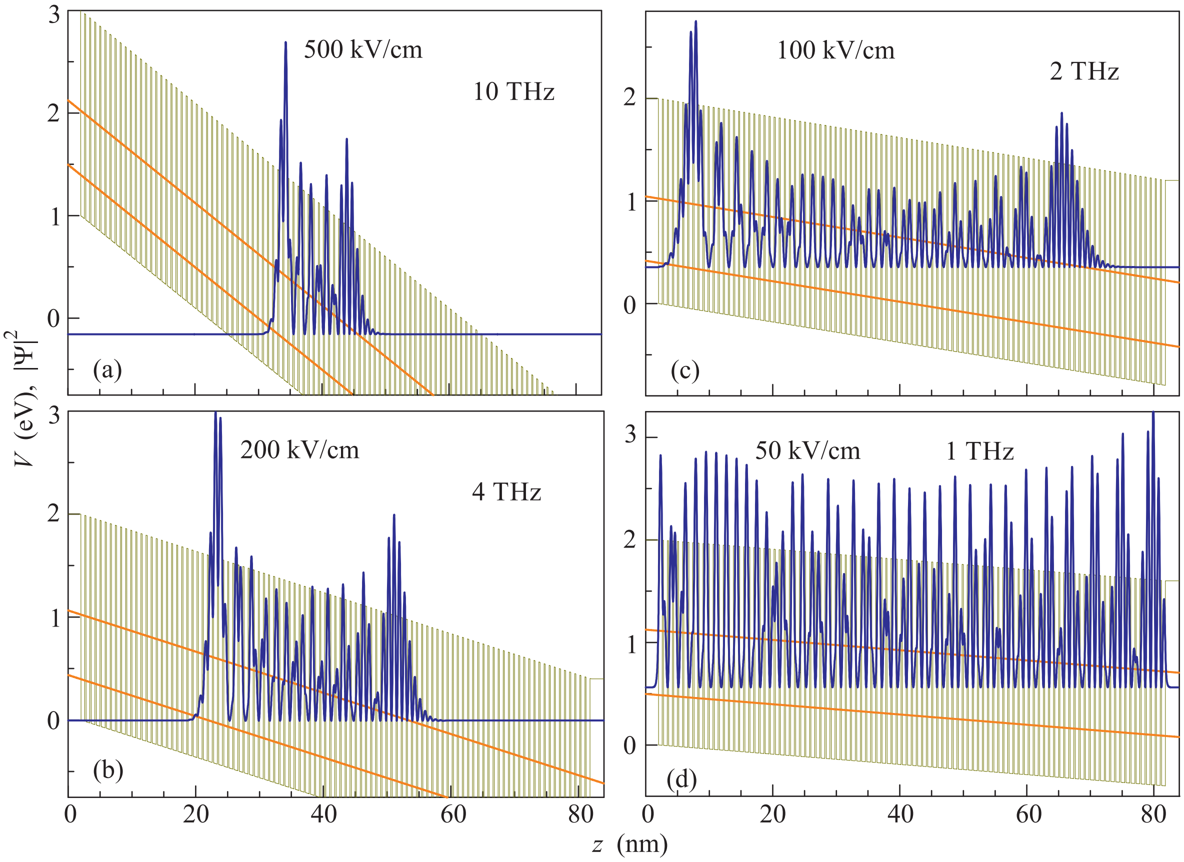

Fig. 4. (Color online) The profile of the potential in biased superlattice and probability density $|\Psi|^2$ for the Stark states. Applied electric field 500 kV/cm corresponding to Bloch frequency 10 THz (a); 200 kV/cm corresponding to 4 THz (b); 100 kV/cm corresponding to 2 THz (c, b); 50 kV/cm corresponding to 1 THz (d). Sloped lines show the boundaries of the miniband

For a field above 100 kV/cm, the Stark states spatially occupy only a fraction of the structure, see Figs. 4a and b. When the magnitude of electric field decreases, Stark states expand, and eventually exceed the size of the structure, and the regime of Wannier–Stark localization becomes replaced by the localization by the barrier which surrounds the structure.

The probability P of the photon spontaneous emission due to radiative transitions between Stark states with energies E_l and E_j is defined by dipole matrix element $\Psi_l|x|\Psi_j$ via Fermi's golden rule:

$$P = \alpha|\langle\Psi_l|x|\Psi_j\rangle|^2 \frac{n^2\omega^3}{\pi c^2}, \tag{4}$$

where $\alpha \approx 1/137$ is a fine structure constant, n is refractive index, $\omega = (E_l - E_j)/\hbar$. An analytical estimate of the dipole matrix element $\langle\Psi_l|x|\Psi_j\rangle$ reads [21, 22]

$$|\langle\Psi_l|x|\Psi_j\rangle| = s/4 \tag{5}$$

and, using Eqs. (1), (3), (4), and (5) the probability of an emission can be estimated as

$$P = \frac{\alpha}{16\pi}\left(\frac{nWd}{c\hbar}\right)^2 \omega. \tag{6}$$

Fig. 5 shows the dependence of the probability of transitions between the neighboring Stark states as a function of BO frequency (which is proportional to applied electric field F, shown in upper scale). As it can be seen, for the frequencies of BO above 2 THz, the probability P is linearly proportional to frequency of emission, and the results of numerical modeling coincide with the analytical estimate obtained using Eq. (6). For frequencies below 2 THz, the size of the Stark state s exceeds the size of the structure, and in this case, the dipole matrix element does not experience a noticeable variation with decreasing applied electric field F. In such a regime, the variation of the probability is governed by the frequency dependence of the density of photonic states (see Eq. (4)), and is proportional to ω^3.

It can also be seen, that the probabilities of transitions over one and over two Stark states (accompanied by emission of radiation with a double and triple Bloch frequency, respectively) have substantial values, and are

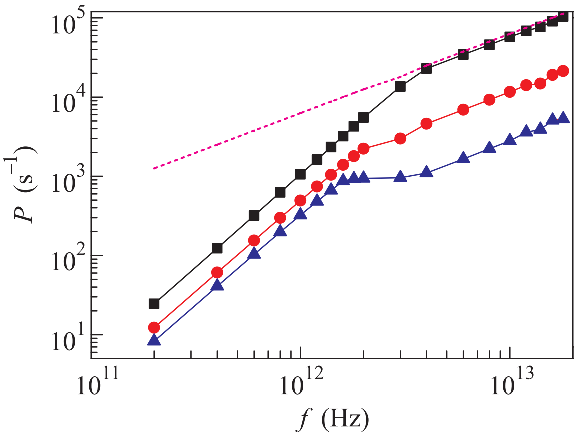

Fig. 5. (Color online) Dependence of the rate of the radiative transition on the frequency of emitted radiation corresponding to the transition between neighboring states separated by single Bloch energy (green squares). Dashed lines show the dependence obtained by analytical Eq. (6). Red circles and blue triangles show the dependence for the transition over one Stark state (between the states separated by double Bloch energy) and over two Stark states (between the states separated by triple Bloch energy). The upper scale shows the value of electric field applied to SL

about an order of magnitude smaller, than the probability of an emission of radiation with the Bloch frequency.

As mentioned in the Introduction, the opening of a minigap in a miniband could lead to coexistence of BO with two different periods and the emission of radiation with a single and double frequency BO. However, the qualitative analysis, leading to such an assumption, operates on the terms associated with the band structure: such the wavevector, Brillouin zone, etc. In reality, in the case of the high electric field required for Wannier–Stark localization, the wavevector is not a good quantum number anymore. Therefore, an intuitive hypothesis about coexistence of BO with two spatial periods require rigorous numerical confirmation.

For the quantitative analysis of the influence of a minigap on BO in the framework of a 1D model, one should superimpose an additional periodic potential (denoted as U in Fig. 2c) to potential $U_{4\mathrm{H}}$. In the subsequent modeling, we will use the width of such a minigap as an independent parameter, in order not to limit our studies to case of silicon carbide but instead to generalize it to an arbitrary SL with a superimposed potential.

When the width of the miniband is small, electrons will tunnel through it without a noticeable reflection – the minigap does not affect the motion of electron. On other hand, when minigap is large, electrons are reflected, and instead of one Stark ladder, two independent Stark ladders occur, as demonstrated in Figs. 1b and 6. There are the states localized in lower Stark ladder (denoted as $|\alpha\rangle$, $|\beta\rangle$, $|\gamma\rangle$) and the states, localized at upper Stark ladder (denoted as $|A\rangle$ and $|B\rangle$). Note that the energies of the Wannier–Stark states in two ladders could be shifted with respect to energies of the state, in the single Stark ladder, formed in miniband with no minigap. Let us define the shift of energy levels δ as $\delta = E_A - (E_a - \hbar\omega)$, $\omega_+ = \omega + \delta$, and $\omega_- = \omega - \delta$. It could be seen, that the energy intervals between the states can have the following different values: $\hbar\omega_+$, $\hbar\omega_-$, $2\hbar\omega$, $\hbar(2\omega + \omega_+)$, and $\hbar(2\omega + \omega_-)$, as explained in the Table 1. In the subsequent discussion, we will use the following notation: the transition between state $|\alpha\rangle$ and state $|A\rangle$ will be described as transition αA, and so on. The value of energy shift δ non-monotonically depends on the width of minigap Δ, as illustrated in Fig. 7a.

Table 1 Possible transitions between the states in biased split miniband shown in Fig. 1b, the frequency of emitted radiation, associated with specific transition

Transition	Frequency of emitted radiation
αA	ω_-
βA	ω_+
$\alpha\beta$	2ω
AB	2ω
αB	$2\omega + \omega_-$
γA	$2\omega + \omega_-$

Fig. 6 shows the profiles of the Stark states for different values of the minigap. An applied electric field of 500 kV/cm corresponds to a Bloch oscillation with a frequency of 10 THz in a SL with no minigap. For comparison, the Stark states in the miniband without minigap are also shown (Fig. 6a). In the case of the absence of a minigap, the energy interval between consecutive states is equal to the Bloch energy, and the profiles of the states are identical. When the minigap appears, two types of Stark states appear, as shown in Figs. 6b–d. The energy interval between the states of different types is either $\hbar\omega_+$, or $\hbar\omega_-$, the interval between the states of the same type is $2\hbar\omega$. When the minigap is large enough (Fig. 6d) the states are distinguishably localized in either upper or lower sub-miniband. When the minigap is small, the Stark states are spread between the two sub-minibands.

The results of numerical modeling of the probabilities of emission caused by various transitions between states in upper and lower miniband are shown in Fig. 7b. It can be seen, that an increase of the width of minigap Δ leads to a decrease of the probability of transitions αA and βA, accompanied by emission of radiation with "single Bloch frequency" ω_+ or ω_-. At the same time, the

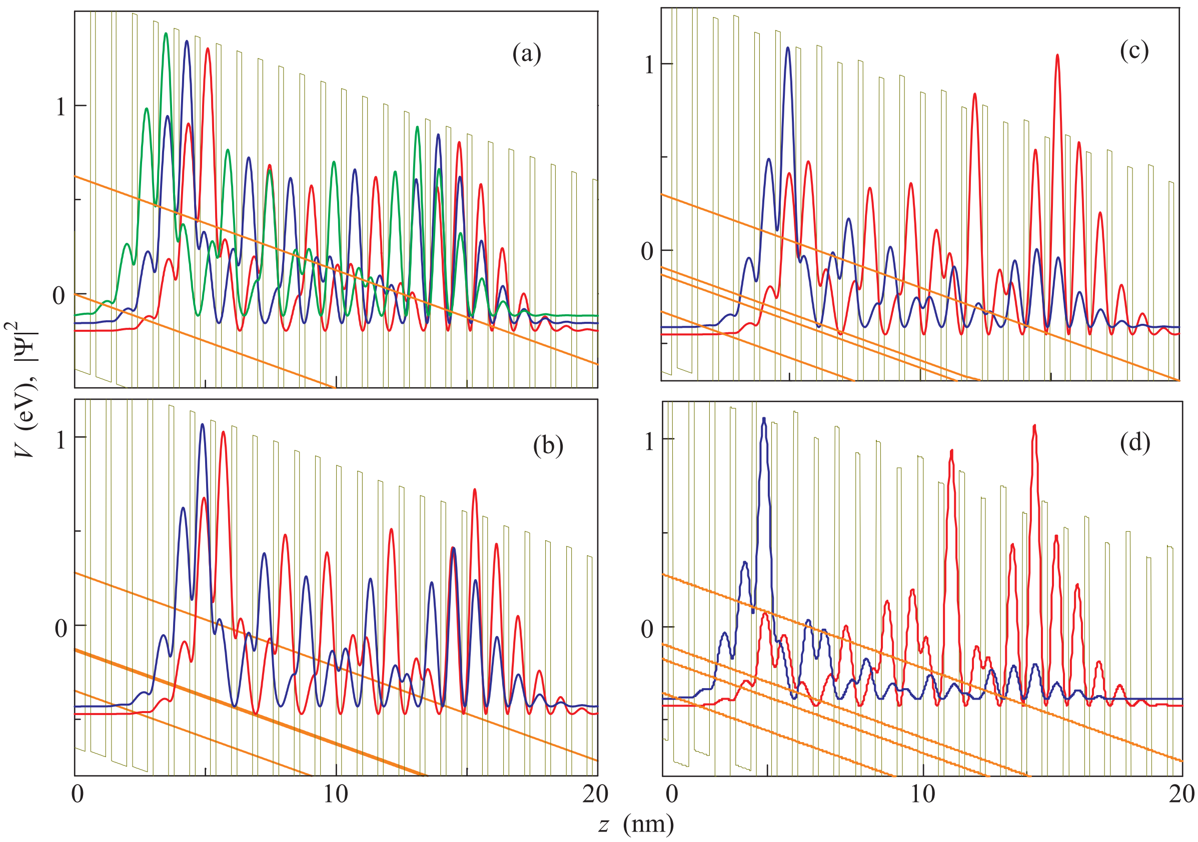

Fig. 6. (Color online) (a) – The profile of the potential in biased superlattice and probability density $|\Psi|^2$ of the three neighboring Stark states in the case of absence of minigap. (b–d) – The profile of the potential in biased superlattice and the probability density $|\Psi|^2$ for the Stark state the type α (blue curve) and of the type A (red curve) in split miniband. Sloped line shows the boundaries of the sub-minibands. Applied electric field is 500 kV/cm, which in the case of absence of the gap corresponds to Bloch frequency 10 THz. The values of minigap are 9 meV (b); 40 meV (c); and 80 meV (d). Sloped orange lines show the boundaries of the minibands

probability of transition at double BO, such as $\alpha\beta$ and AB, demonstrates non-monotonic behavior and, when the width of minigap exceeds 30 meV, the probability of transitions $\alpha\beta$ becomes comparable to the probability related to the single Bloch frequency. It means that the spectrum of emission caused by Bloch oscillations could be substantially modified: an additional emission line at double the Bloch frequency can appear, and the width of the line at the Bloch frequency could be increased due to a shift of energy levels in two Stark ladders. Note that for the 1D model potential considered here, a noticeable influence on the minigap occurs only when the width of the minigap Δ exceeds Bloch energy given by Eq. (1).

To conclude, we have shown that Bloch oscillations are anharmonic: it could be accompanied by emission of radiation with double, triple and, in general, multiples of the Bloch frequency. We have also analyzed the influence of the minigap on the Bloch oscillation process, and have shown that, in this case, two independent Stark ladders appear and the energies of the Stark states in the upper and lower ladders are shifted with respect to each other. The predicted effects can lead to an increase of intensity at double the frequency of Bloch oscillation, and a broadening of the emission line at the single frequency of Bloch oscillation.

Authors thank V.I. Sankin and A.V. Andrianov for useful discussion. A.J.G. acknowledges support by FP7 IRSES project POLATER and FP7 ITN project NOTEDEV.

Appendix. Eigen energies of Stark states and their corresponding wavefunctions have been obtained by solving the Schrödinger equation by the transfer matrix technique using outgoing wave boundary conditions [24], implying that no wave is incident on the structure from outside. In the basis of propagating wave transfer matrix through a uniform layer of the thickness d_i is given by

$$\hat{M}_i = \begin{pmatrix} \exp(ik_i d_i) & 0 \\ 0 & \exp(-ik_i d_i) \end{pmatrix}, \qquad (7)$$

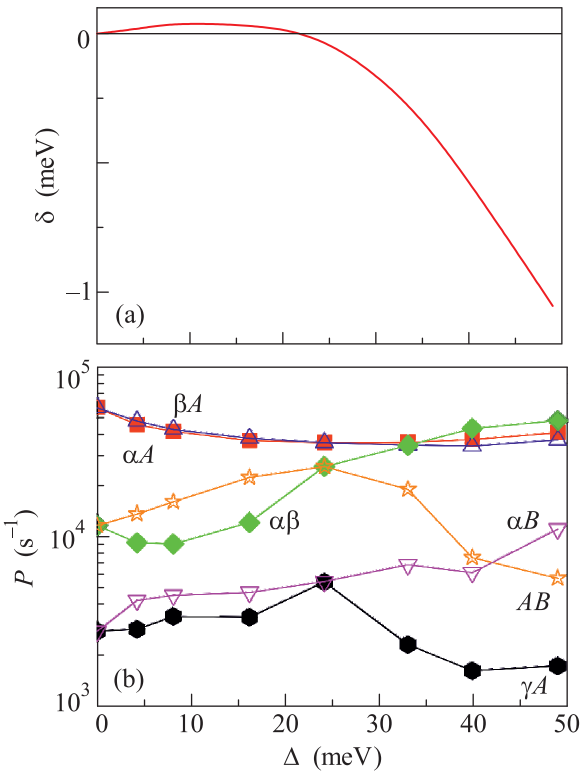

Fig. 7. (Color online) (a) – The dependence of the energy shift between lower and upper Stark ladders on the width of the minigap Δ. (b) – The probabilities of the radiative transitions at "single" Bloch energy (αA and βA), double Bloch energy ($\alpha\beta$ and AB), and "triple" Bloch energy (αB and γA), as a function of the width of minigap Δ

where wavevector $k_i = \sqrt{2m_i(E-U_i)}/\hbar$, m_i is an effective mass of an electron, E is an energy of eigenstate, and U_i is the potential energy of an electron. The transfer matrix through the interface between layers with indices i and $i+1$ reads

$$\hat{T}_i = \frac{1}{2}\begin{pmatrix} 1+\dfrac{m_{i+1}k_i}{m_i k_{i+1}} & 1-\dfrac{m_{i+1}k_i}{m_i k_{i+1}} \\ 1-\dfrac{m_{i+1}k_i}{m_i k_{i+1}} & 1+\dfrac{m_{i+1}k_i}{m_i k_{i+1}} \end{pmatrix}. \tag{8}$$

The transfer matrix through the whole structure $\hat{M}$ is the product of the transfer matrices through individual layers and boundaries between them. An equation for eigenenergies can be obtained by coupling of the amplitudes of outgoing wave on the right and left sides of the structure:

$$A\begin{pmatrix} 1 \\ 0 \end{pmatrix} = \hat{M}(E)\begin{pmatrix} 0 \\ 1 \end{pmatrix}, \tag{9}$$

where A is some constant. Eventually, an equation for the energies of a localized eigenstate can be reduced to the simple form

$$M_{22}(E) = 0. \tag{10}$$

In the case of biased periodic potential Eq. (10) gives the set of equidistant E_j, and the interval between neighboring states is equal to the Bloch energy: $|E_{j+1}-E_j| = eFd$.

Wavefunctions Ψ_i of localized Stark states with energy E_j can be obtained by the transfer matrix technique.

---

1. F. Bloch, Z. Phys. **52**, 555 (1928).
2. C. Zener, Proc. R. Soc. London, Ser. A **145**, 523 (1934).
3. K. Leo, Semicond. Sci. Tech. **13**, 249 (1998).
4. P. Voisin, Ann. Phys. Fr. **22**, 681 (1997).
5. G.H. Wannier, Phys. Rev. **117**, 432 (1960).
6. H.M. James, Phys. Rev. **76**, 1611 (1949).
7. L. Esaki and R. Tsu, IBM J. Res. Dev. **14**, 61 (1970).
8. A. Sibille, J.F. Palmier, H. Wong, J.C. Esanault, and F. Mollot, Phys. Rev. Lett. **64**, 52 (1990).
9. F. Beltram, F. Capasso, D.L. Sivco, A.L. Hutchinson, S.N.G. Chu, and A.Y. Cho, Phys. Rev. Lett. **64**, 3167 (1990).
10. R. Terazzi, T. Gresch, M. Giovannini, N. Hoyler, N. Sekine, and J. Faist, Nat. Phys. **3**, 329 (2007).
11. P.G. Savvidis, B. Kolasa, G. Lee, and S.J. Allen, Phys. Rev. Lett. **92**, 196802 (2004).
12. P. Voisin, J. Bleuse, C. Bouche, S. Gaillard, C. Alibert, and A. Regreny, Phys. Rev. Lett. **61**, 1639 (1988).
13. E.E. Mendez, F. Agullo-Rueda, and J.M. Hong, Phys. Rev. Lett. **60**, 2426 (1988).
14. C. Waschke, H.G. Roskos, R. Schwedler, K. Leo, and H. Kurz, Phys. Rev. Lett. **70**, 3319 (1993).
15. Y. Shimada, K. Hirakawa, M. Odnoblioudov, and K.A. Chao, Phys. Rev. Lett. **90**, 046806 (2003).
16. L.S. Ramsdell, Am. Miner. **32**, 64 (1947).
17. A.R. Verma and P. Krishna, *Polymorphism and Polytypism in Crystals*, Wiley, N.Y. (1966).
18. V.I. Sankin and I.A. Stolichnov, Superlatt. and Microstruct. **23**, 999 (1998).
19. V.I. Sankin, A.V. Andrianov, A.G. Petrov, and A.O. Zakhar'in, Appl. Phys. Lett. **100**, 111109 (2012).
20. A. Laref and S. Laref, Phys. Stat. Sol. B **245**, 89 (2008).
21. M. Luban, J. Math. Phys. **26**, 2386 (1985).
22. A.M. Bouchard and M. Luban, Phys. Rev. B **52**, 5105 (1995).
23. D. Cai, A.R. Bishop, N. Gronbech-Jensen, and M. Salerno, Phys. Rev. Lett. **74**, 1186 (1995).
24. S. Winnerl, E. Schomburg, S. Brandl, O. Kus, K.F. Renk, M.C. Wanke, S.J. Allen, A.A. Ignatov, V. Ustinov, A. Zhukov, and P.S. KopTev, Appl. Phys. Lett. **77**, 1259 (2000).

25. K. Hofbeck, J. Grenzer, E. Schomburg, A. A. Ignatov, K. F. Renk, D. G. Pavel'ev, Yu. Koschurinov, B. Melzer, S. Ivanov, S. Schaposchnikov, and P. S. Kop'ev, Phys. Lett. **218**, 349 (1996).
26. G. B. Dubrovskii, Sov. Phys. Sol. Stat. **13**, 2107 (1972).
27. G. B. Dubrovskii and A. A. Lepneva, Sov. Phys. Sol. Stat. **19**, 1252 (1977).
28. G. B. Dubrovskii, A. A. Lepneva, and E. I. Radovanova, Phys. Stat. Sol. B **57**, 423 (1973).
29. V. I. Sankin, A. G. Petrov, and M. A. Kaliteevski, J. Appl. Phys. **114**, 063704 (2013).
30. M. A. Kaliteevski, D. M. Beggs, S. Brand, R. A. Abram, and V. V. Nikolaev, Phys. Rev. B **73**, 033106 (2006).